Wearable Finger Tracking and Cutaneous Haptic Interface with Soft Sensors for Multi-Fingered Virtual Manipulation

Yongjun Lee, Myungsin Kim, Yongseok Lee, Junghan Kwon, Yong-Lae Park, and Dongjun Lee

***Abstract*—Multi-Fingered haptics is imperative for truly immersive virtual reality experience, as many real-world tasks involve finger manipulation. One of the key lacking aspect for this is the absence of technologically and economically viable wearable haptic interfaces that can simultaneously track the finger/hand motions and display multi-degree-of-freedom (DOF) contact forces. In this paper, we propose a novel wearable cutaneous haptic interface (WCHI), which consists of 1) finger tracking modules (FTMs) to estimate complex multi-DOF finger and hand motion; and 2) cutaneous haptic modules (CHMs) to convey three-DOF contact force at the finger-tip. By opportunistically utilizing such different types of sensors as inertial measurement units, force sensitive resistor sensors, and soft sensors, the WCHI can track complex anatomically consistent multi-DOF finger motion while avoiding FTM-CHM electromagnetic interference possibly stemming from their collocation in the small form-factor interface; while also providing the direction and magnitude of three-DOF finger-tip contact force, the feedback of which can significantly enhance the precision of contact force generation against variability among users via their closed-loop control. Human subject study is performed with a virtual peg insertion task to show the importance of both the multi-DOF finger tracking and the three-DOF cutaneous haptic feedback for dexterous manipulation in virtual environment.**

***Index Terms*—Cutaneous haptic feedback, finger motion tracking, soft sensors, virtual reality (VR), wearable haptic interface.**

I. Introduction

With the recent advents of many commercial head-mounted displays (e.g., Oculus Rift, HTC VIVE, GearVR) along with the developments in onboard computing, sensing and sensor fusion, communication, and microelectromechanical systems (MEMS) sensor and actuator technologies, in recent years, wearable haptics for virtual reality (VR) have received great attention and been under active investigation by many research groups and companies around the globe. Among many forms of wearable haptics, particularly promising is the multi-finger-based wearable haptics, since it allows for the VR realization of many real-life scenarios and interactions, which typically involve heavy usage of fingers and hands. In fact, using the fingers and hands is argued as one of the key characteristics of our human being itself; thus, we believe that finger-based wearable haptics is crucial to attain truly immersive, multifarious, and real-life like VR experiences.

For this finger-based wearable haptics for VR, the first requirement is reliable tracking of multiple fingers and hands in various motions and postures. Many methodologies have been proposed for this multi-finger tracking. Vision-based technology (e.g., Kinect, LeapMotion, [1]–[4]) has attracted many researchers in recent years, since it can be used with bare hands. However, it fundamentally suffers from the occlusion problem, which is unavoidable for VR scenarios whenever it involves dexterous fingers/hand movements. Further, it often fails to track the fingers when some extra devices (e.g., haptic device [5]) are attached on them. Soft sensor-based technology (e.g., Cyber Gloves [6], [7]–[10]) has been investigated for its ease of implementation in the form of wearable gloves. However, it typically has only single-degree-of-freedom (DOF) motion sensing capability per the sensor, thus, to estimate large-DOF finger/hand motion, it necessitates complex arrangement of "pack" of many of them wrapping around the fingers/hand, and, consequently, complicated calibration algorithm. The inertial measurement unit (IMU) based technology (e.g., Perception Neuron [11], [12]–[14]) has been studied with its advantage of providing the global three-DOF orientation information at once along with its relatively flexible sensor attachment location. However, its susceptibility to electromagnetic interference limits its applica-

Manuscript received January 21, 2018; revised June 17, 2018; accepted September 14, 2018. Date of publication October 9, 2018; date of current version February 14, 2019.Recommended by Technical Editor Prof. J. Ueda. This work was supported by the Global Frontier R&D Program (2013M3A-6A3079227), by the Engineering Research Center Program for Soft Robotics (2016R1A5A1938472) all through the National Research Foundation funded by MSIT, South Korea, and also by the Industrial Strategic Technology Development Program (10060070) funded by MOTIE, South Korea. *(Corresponding author: Dongjun Lee.)*

Y. Lee was with the Department of Mechanical and Aerospace Engineering and IAMD, Seoul National University, Seoul 08826, South Korea and is current with the HARNICS, Seoul 08501, South Korea (e-mail: yongjun@harnics.com).

M. Kim, Y. Lee, J. Kwon, Y.-L. Park, and D. Lee are with the Department of Mechanical and Aerospace Engineering and IAMD, Seoul National University, Seoul 08826, South Korea (e-mail: myungsinkim@snu.ac.kr; yongseoklee@snu.ac.kr; jhkwon@snu.ac.kr; ylpark@snu.ac.kr; djlee@snu.ac.kr).

This paper has supplementary downloadable material available at http://ieeexplore.ieee.org provided by the authors.

Color versions of one or more of the figures in this paper are available online at http://ieeexplore.ieee.org.

Digital Object Identifier 10.1109/TMECH.2018.2872570

1083-4435 © 2018 IEEE. Translations and content mining are permitted for academic research only. Personal use is also permitted, but republication/redistribution requires IEEE permission. See http://www.ieee.org/publications_standards/publications/rights/index.html for more information.

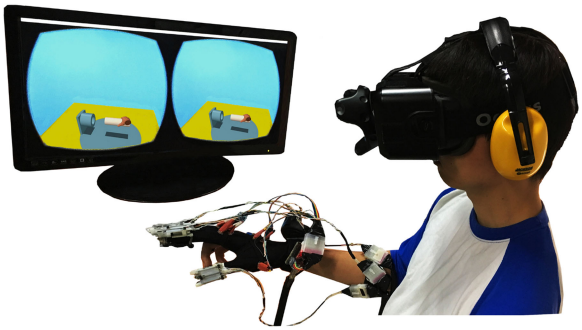

Fig. 1. Multi-fingered virtual manipulation with the WCHI: a peg insertion task into a horizontally placed hole.

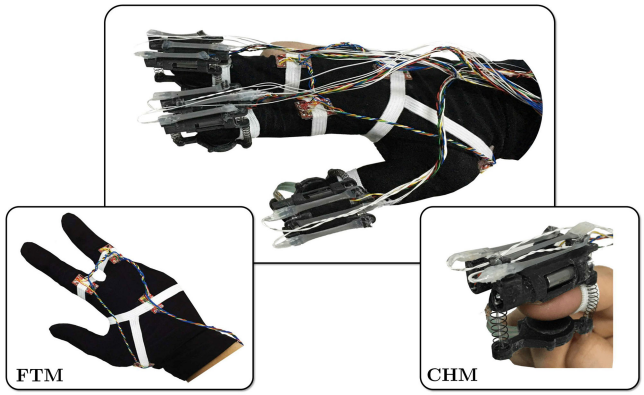

Fig. 2. WCHI with FTM and CHM: 1) IMUs and soft sensors are opportunistically utilized for FTM; 2) three-DOF finger-tip force provided by CHM with soft sensors and FSR sensor; and 3) FTM and CHM designed with minimal mechanical/functional interference for their easy integrated (and also separate) usage.

bility, particularly when it is required to be physically collocated with actuators as for the case of wearable finger-based haptics (e.g., [13], [15]).

Along this reasoning, in this paper, we propose a novel glove-type *finger tracking module* (FTM), which opportunistically utilizes IMU sensors and soft sensors to estimate multi-DOF finger/hand motion while being free from the electromagnetic interference issue of the IMUs and the complex sensor wrapping/arrangement issue of the soft sensors. The proposed FTM is designed in the simple glove-form for easy integrated (or separate) usage with haptic devices and straightforward implementation. We determine the attaching locations of each sensor to minimize the system complexity while also carefully observing the finger/hand anatomy and considering different sensing capabilities and characteristics of each sensor. Our proposed FTM also only requires a simple three-step known-pose-based calibration. Section II contains the design and algorithms for this FTM.

On top of the finger/hand tracking, haptic feedback is also imperative for immersive VR experiences. For this, cutaneous haptic feedback (with skin deformation) has received wide attention for wearable finger-based haptics for its portability, small form-factor, and affordability as compared to kinesthetic haptic feedback (e.g., Sensable Phantom) and also its ability to supplement or even substitute the kinesthetic feedback [16]–[18]. Various finger-tip cutaneous haptic devices have been proposed (e.g., [19]–[23]). A two-DOF band-driven cutaneous device was proposed in [19], and later adopted in [20] and extended to a three-DOF wire-driven module [21]. The work of Prattichizzo *et al.* [21] attached three force sensitive resistor (FSR) sensors on a contact plate and use their readings to estimate the pose of the plate to generate three-DOF haptic feedback. For this, they utilized human finger-tip stiffness model and also required continuous contact with all the three FSR sensors, both compromising robustness of the device. To circumvent this issue of (indirect) pose estimation, a device with mechanical linkage was proposed in [22] and [23] with the position control used to generate haptic feedback. These linkage-devices of [22] and [23], however, are much bulkier than wire-based cutaneous devices and still suffer from the robustness issue, since they also relied on human finger-tip stiffness model to generate haptic feedback from the position control.

To retain portability, affordability, and small form-factor while also improving robustness, in this paper, we develop a novel a wire-driven type *cutaneous haptic module* (CHM) capable of providing three-DOF finger-tip force. The actuation mechanism is similar to that in [21]. The key differentiating aspect is our adoption of closed-loop control strategy based on the feedback of direct measurement instead of some human models with inevitable uncertainty and interuser variability. For this, we utilize soft sensors and FSR sensor to directly measure the magnitude and direction of the finger-tip force, and feedback that in the form of proportional-integral (PI) control to generate high-performance three-DOF finger-tip haptic feedback, which is also robust against uncertainty, friction, unmodeled compliance, and user variability. Section III contains the design, estimation, and control algorithms for this CHM.

Combining these FTM and CHM, we construct our proposed wearable cutaneous haptic interface (WCHI) (see Fig. 1 for this WCHI in use and Fig. 2 for its construction). Most closely related to our WCHI are the work of Weber *et al.* [24] and MANUS VR glove [25], both providing finger tracking and haptic feedback simultaneously with IMUs and soft sensor adopted. However, 1) the device of Weber *et al.* [24] utilizes only a single IMU on the dorsum of the hand and a single soft sensor for each finger, thus, not able to fully track large-DOF complex finger motions; 2) MANUS VR glove [25] can fully track the thumb motion, yet, not the adduction-abduction (AA) motion of index/middle fingers, which turns out to substantially affect VR experience, particularly it involves complex/dexterous finger motion (see Section IV-B); and 3) both of these devices provide only single-DOF vibro-tactile feedback on the finger-tip, too simple to capture most of real-life finger/hand interactions. In contrast to this, our proposed WCHI can fully track complex/dexterous large-DOF finger/hand motions including the finger AA motion, while also providing three-DOF cutaneous finger-tip haptic feedback with performance/robust feedback control. The FTM and CHM are also designed in such a way that they can be easily integrated into the WCHI without mechanical and functional interferences (e.g., electromagnetic interference) or used separately.

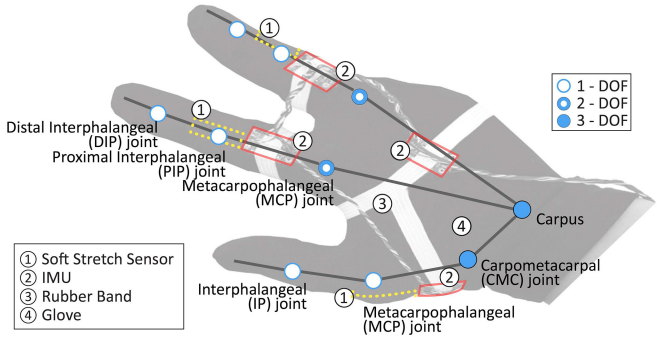

Fig. 3. FTM consists of IMUs and soft sensors embedded in the form of glove (hand model with links and joints also illustrated).

The rest of the paper is organized as follows. Sections II and III contains the design, development, analysis, and algorithms of the FTM and CHM. Section IV presents the integrated WCHI combining the FTM and CHM and the results of human subject study to verify the performance of the proposed WCHI. Section V concludes the paper with some comments on future research direction.

II. Development of Finger Tracking Module

A. Hardware Set-Up of the FTM

The two key challenges of vision-based multi-fingered tracking are: 1) the finger motion has large-DOF motion within a small region, thus, such commercial systems as HTC VIVE, Kinect or VICON, which can fairly well track "larger" arm or wrist motions, cannot be directly used; and 2) the dexterous finger motion, combined with omnidirectional wrist motion, frequently induces the issue of occlusion, which is fundamental for any vision-based systems (e.g., LeapMotion) and has not yet been overcome. Due to these reasons, in this paper, we aim to develop FTM with IMUs and soft sensors, all attached in the glove form, so that large-DOF/small-size finger motion can be tracked while avoiding the issue of occlusion. See Fig. 3, where we assume the wrist position information is provided by a commercial external vision sensor (e.g., HTC VIVE) and also anatomical constants (i.e., link length, joint position, etc.) given from offline identification (e.g., [26]). The FTM fully tracks each segment of the thumb, index, and middle fingers. To determine which sensor is attached to which segment, we carefully consider the DOF of each joint, which varies from one to three.

More precisely, we decide the joints, the finger segments, and the sensor arrangement for the FTM as shown in Fig. 3, where 1) hand dorsum/carpus is with three-DOF rotation (e.g., wrist rotation); 2) three-DOF carpometacarpal (CMC) joint with flexion-extension (FE), pronation-supination (PS), and abduction-adduction (AA) motions; and 3) two-DOF metacarpophalangeal (MCP) joint of the index/middle fingers with FE and AA motions. To estimate the (relative) orientations of these joints with a single sensor attachment, we attach four MEMS IMUs (InvenSesne MPU9250) on the dorsum of the hand, on the first metacarpal of the thumb, and the proximal phalanges of the index and middle fingers, respectively. We choose these IMUs over soft sensors here, since 1) they can provide three-DOF global rotation information at once; and 2) their attachment point is more flexible than soft sensors, that must be attached wrapping over the joint. These IMUs are fastened by rubber bands in the form of glove. We also attach the IMUs as far from the finger-tip CHM as possible to avoid electromagnetic interference between the motors of CHMs and the magnetometers of the IMUs (see Section IV for interference test result). On the other hand, we utilize three capacitive type soft sensors (StretchSense) and embed them inside the glove of each finger, to estimate the single-DOF bending angles of the thumb MCP joint and the proximal interphalangeal (PIP) joints of the index/middle fingers. Here, we consider the thumb MCP joint to be single-DOF with the FE motion, since its AA motion caused by its interconnection with the CMC joint is relatively small [27], [28] especially during the finger grasping and manipulation.

In addition, we utilize the musculoskeletal dependency (i.e., synergy) to estimate the motion of the thumb interphalangeal (IP) joint and distal IP (DIP) joints of the index/middle fingers from the thumb MCP joint and index/middle finger PIP joints. Note that we utilize the synergy not only for index/middle fingers, but also for the thumb. This synergy was investigated in [29] and later employed in [13]. Hrabia *et al.* [29] showed that the synergy of the thumb MCP joint ($R^2 = 0.59$) is weaker than that of index finger's DIP joint ($R^2 = 0.77$), yet, still similar to that of little finger ($R^2 = 0.63$). In this paper, we adopt this thumb synergy with its strength determined by trial-and-error, which turns out to be adequate for our purpose, that is, the FTM for VR applications, where believable graphics and haptic sensations are enough as evidenced/illustrated through our (rather extensive) experiments (see Section IV) in contrast to, e.g., medical applications, where accuracy is more weighted. Utilizing the soft sensors and the synergies for single-DOF joints and IMUs for multi-DOF joints, we can reduce the number of the sensor attachments, resulting in simpler estimation algorithm and lesser electromagnetic interference when integrated with the CHM.

In this paper, we use five-DOF thumb model with single-DOF IP/MCP joints and three-DOF CMC joints. This is slightly different from the more typical five-DOF thumb model, which is employed for robot hand design, where single-DOF for the IP joint and two-DOF for the MCP and CMC joints are used [30], [31]. The advantage of our modeling is that we can fully incorporate the three-DOF CMC motion of the thumb with their axes not intersecting [26], [32] while utilizing a few number of sensors. This five-DOF thumb model also turns out to provide graphically and haptically plausible sensations through our experiments, including multi-user subject study.

B. Finger/Hand Pose Estimation for the FTM

1) Tracking Algorithm of the FTM: To estimate the configuration of FTM (i.e., poses of three fingers and hand), we apply the forward kinematics to each joint of the fingers and the hand. Let $p^s_{s,h} \in \Re^3$ be the position vector from the origin of the inertial frame $\{s\}$ to that of the hand frame $\{h\}$ expressed in $\{s\}$-frame, where $\{h\}$-frame is attached to the hand dorsum as shown in

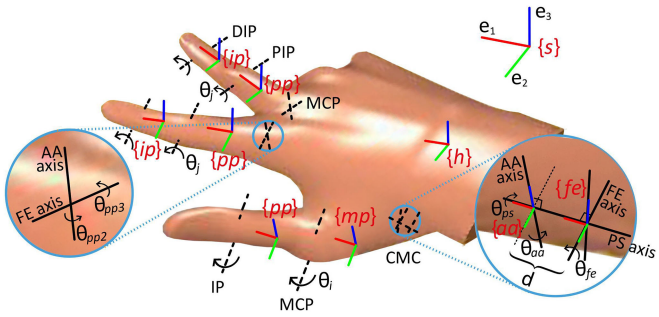

Fig. 4. Hand model with the joints, links, and coordinate frames: thumb possesses three-DOF CMC joint, single-DOF MCP and IP joints; whereas index and middle fingers each possesses two-DOF MCP joint, single-DOF PIP and IP joints.

Fig. 4. In this paper, we use an external low-cost vision sensor (e.g., HTC VIVE tracker) to measure this $p^s_{s,h}$. Denote the pose of the $\{h\}$-frame relative to the $\{s\}$-frame by the homogeneous transformation $\bar{g}^s_{s,h} \in \text{SE(3)}$, i.e.,

$$\bar{g}^s_{s,h}(R^s_{s,h}, p^s_{s,h}) = \begin{bmatrix} R^s_{s,h} & p^s_{s,h} \\ 0 & 1 \end{bmatrix} \in \text{SE(3)}$$

where the $R^s_{s,h} \in \text{SO(3)}$ is the rotation of $\{h\}$ w.r.t. $\{s\}$, which is to be measured by the IMU attached to the $\{h\}$-frame as shown in Fig. 4 (e.g., [33]).

Let us consider first the thumb motion. For this, we attach the frames $\{fe\}$ and $\{aa\}$ to the CMC joint and $\{mp\}$ to the metacarpal bone between the MCP and CMC joints to, respectively, express the FE motion θ_{fe}, the PS motion θ_{ps}, and the AA motion θ_{aa} of the CMC joint with the offset among their axes also taken into account—see Fig. 4. We then have the following kinematics of the $\{mp\}$-frame expressed in the $\{s\}$-frame:

$$\bar{g}^s_{s,mp} = \bar{g}^s_{s,h} \cdot \bar{g}^h_{h,mp}(R^h_{h,mp}, p^h_{h,mp}) \in \text{SE(3)} \tag{1}$$

with

$$R^h_{h,mp} = R^h_{h,fe} R^{fe}_{fe,aa} R^{aa}_{aa,mp} = R^{s,T}_{s,h} R^s_{s,mp} \tag{2}$$
$$p^h_{h,mp} = p^h_{h,fe} + R^h_{h,fe} p^{fe}_{fe,aa} + R^h_{h,aa} p^{aa}_{aa,mp}$$

where $R^h_{h,fe} = \exp(\theta_{fe} e_2)$, $R^{fe}_{fe,aa} = \exp(\theta_{ps} e_1)$, and $R^{aa}_{aa,mp} = \exp(\theta_{aa} e_3)$ with the corresponding frames initially aligned with each other, $R^h_{h,aa} = R^h_{h,fe} R^{fe}_{fe,aa}$, $\exp(\cdot)$ the exponential map [34], and $e_i \in \Re^3$ the unit basis vector; and $p^h_{h,fe}, p^{fe}_{fe,aa}$ and $p^{aa}_{aa,mp}$ are the anatomical lengths, which are assumed constant and known with $p^{fe}_{fe,aa} = de_1 = [d; 0; 0]$ (i.e., offset d along the PS motion axis—see Fig. 4. Here, with the IMU sensors attached to the $\{h\}$-frame and the $\{mp\}$-frame (see Fig. 3), we can directly measure $R^s_{s,h}$ and $R^s_{s,mp}$, and, consequently, $R^h_{h,mp}(\theta_{fe}, \theta_{ps}, \theta_{aa})$ from (2). By solving the inverse kinematics for $R^h_{h,mp}(\theta_{fe}, \theta_{ps}, \theta_{aa})$ with θ_{fe}, θ_{ps}, and θ_{aa} being the pitch, roll, and yaw angles, we can decode $(\theta_{fe}, \theta_{ps}, \theta_{aa})$ from $R^h_{h,mp}$ [34], which are then in turn used to compute the full thumb posture. In this paper, $(p^h_{h,fe}, p^{fe}_{fe,aa}, p^{aa}_{aa,mp})$ (and similar length parameters) are also offline tuned to produce graphically plausible motion during all of our experiments—how to online calibrate them is a research topic by itself and a topic of our future research as well.

Algorithm 1: Three-Step Calibration Procedure of the FTM.

1: Align the direction of the tip of each index/middle finger and hand while keep them straight (i.e., $\theta_i = 0°$).
2: Align the direction of the tip of the thumb to be parallel to the direction of the step 1 while keep it straight.
3: Bend each PIP joint of the index/middle fingers and MCP joint of the thumb to be 90°.

On the other hand, to describe the posture of the index and middle fingers, we attach the $\{fe\}$-frame and $\{aa\}$-frame to the two-DOF MCP joint and the $\{pp\}$-frame to the proximal phalange as shown in Fig. 4. Then, similar to (1) with $R^{fe}_{fe,aa} = I$ and $d = 0$ (i.e., $\{fe\}$-frame is the same as $\{aa\}$-frame for the MCP joint), we can obtain the following kinematics similar:

$$\bar{g}^s_{s,pp} = \bar{g}^s_{s,h} \cdot \bar{g}^h_{h,pp}(R^h_{h,pp}, p^h_{h,pp})$$

where

$$R^h_{h,pp} = R^h_{h,fe} R^{fe}_{fe,pp} = R^{s,T}_{s,h} R^s_{s,pp}$$
$$p^h_{h,pp} = p^h_{h,fe} + R^h_{h,fe} p^{fe}_{fe,pp}$$

where $R^s_{s,h}$ and $R^s_{s,pp}$ are measured by the IMU sensors attached, respectively, to the $\{h\}$-frame and the $\{pp\}$-frame, $R^h_{h,fe} = \exp(\theta_{fe} e_2)$ and $R^{fe}_{fe,pp} = \exp(\theta_{aa} e_3)$ with $(\theta_{fe}, \theta_{aa})$ decodable via the inverse kinematics of $R^h_{h,pp}(\theta_{fe}, \theta_{aa})$ similar for the thumb motion. Finally, for the MCP joint of the thumb or PIP joint of the index/middle fingers, one soft sensor is attached to provide the angle measurement θ_i or θ_j (along the e_2-direction). We can then obtain $\bar{g}^{mp}_{mp,pp}$ or $\bar{g}^{pp}_{pp,ip}$ with $R^{mp}_{mp,pp} = \exp(\theta_i e_2)$ or $R^{pp}_{pp,ip} = \exp(\theta_j e_2)$ and $p^{mp}_{mp,pp}$ or $p^{pp}_{pp,ip}$, with which we can complete the posture estimation of the thumb/index/middle fingers.

2) Calibration Method of the FTM: Each person has different size/shape of the finger/hand. Thus, the sensor attachments would be all different among different users, even if they wear the same FTM. To solve this issue, we perform a known-pose-based sensor calibration. First, the soft sensor has a linear relationship between the relative joint angle and its measurement $\rho_i \in \Re$, i.e.,

$$\theta_i = \beta_0 + \beta_1 \rho_i$$

where $\beta_0, \beta_1 \in \Re$ are coefficients. To find these coefficients, we need to take at least two known poses while measuring ρ_i with corresponding θ_i (e.g., ρ_i at 0° and 90°). On the other hand, the IMU sensors provide orientation information expressed in the $\{s\}$-frame. However, whenever attached to the FTM and worn by the user, their real attachment is unknown and, in general, not the same as the target finger/hand segment as shown in Section II-B1. In other words, for each IMU, we have the following relation:

$$R^s_{s,f} = R^s_{s,b} R^b_{b,f}$$

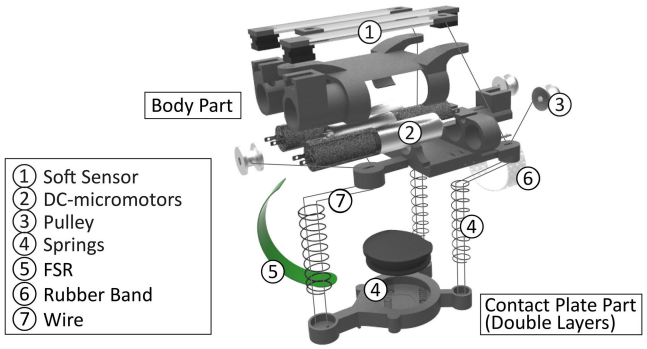

Fig. 5. Hardware design of the CHM for three-DOF cutaneous force feedback consisting of: (a) three dc-micromotors to pull wires with spring support; (b) custom-built soft sensors to measure the wire lengths; and (c) contact plate with tiltable two-layer design and a FSR sensor.

where $R^s_{s,f}, R^s_{s,b}, R^b_{b,f} \in \mathrm{SO}(3)$ are the rotation of the finger/hand segment expressed in the $\{s\}$-frame, the measurement of the IMU, and the misalignment between the finger segment and the IMU sensor frame, respectively. Then, by letting user to assume a known pose, $R^s_{s,f}$ is known, $R^s_{s,b}$ is measured, thus, we can estimate $R^b_{b,f}$. Now, note that the number of unknowns is three (for IMUs) and two (for soft sensors). Thus, if we ask the user to assume three known poses, we can calibrate those three (or two) unknown quantities for each sensor. This is captured by the calibration procedure in Algorithm 1, with the three known postures. See also the supplement video how this three-step calibration is performed.

III. Development of Cutaneous Haptic Module

A. Hardware Set-Up of the CHM

The CHM consists of two parts, (static) *body* part and (moving) *contact plate* part as shown in Fig. 5. Acting as a ground, the body is placed on the finger-tip and rigidly fastened on the distal phalanges of the thumb and index/middle fingers by a rubber band. On the other hands, to deliver the cutaneous haptic sensation, the contact plate is suspended from the body through wires and springs. Three dc-micromotors (Faulhaber®, $\phi = 6$ [mm], 64 : 1 gear ratio) are mounted on the body, one heading forward to finger-tip and other two heading backward so that each motor shaft formalizes vertices of an isosceles triangle. This triangle formation allows the CHM to have a small form factor to be fitted on the limited size of the finger-tip. On each motor shaft, the pulley tied with the wire is rigidly attached, to generate tensile force with the motors. Similar alignment as the motors, three soft sensors are placed on top side of the body to estimate the relative poses between the body and the contact plate. We employ the custom-fabricated resistive type soft sensors [35] for the CHM, rather than the commercial capacitive type soft sensors of the FTM, since it requires very low stiffness to minimize the hindrance of the tensile force from motors and maintain the spring-induced gap between the two parts for the thumb and fingers. In addition, as mentioned in Section II-A, the soft sensors can be robustly utilized with actuators to estimate the configuration of the contact plate.

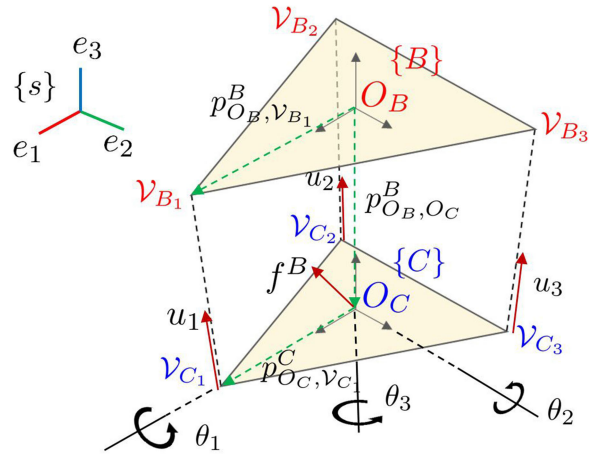

Fig. 6. Configuration and definitions of frames/parameters for the control of CHM.

The contact plate then generates the pushing force at the finger-tip by being pulled through the wires. Its center has a two-layer structure to efficiently estimate the contact force by using only one FSR sensor in any relative rotation between the two parts. The top side of the upper layer is designed to have a concave curvature similar to the volar surface of the finger-tip to increase the contacting area, thus maximizing a sensation by maintaining the contact with finger in any tilted situation. The bottom side of the upper layer has a convex curvature to maintain a continuous contact of the FSR sensor, which is placed at the center of the lower layer.

Between the body and the contact plate, three springs ($k_s = 0.1$ N/mm) are placed to retain a space with no pulling force input. We carefully select the spring length and diameter, 20 and 5 mm, to secure the average ring size of male 18.9 mm and not to cause the buckling problem [36]. Note that the compliance of the custom fabricated soft sensors, the elasticity of the soft sensors has a small influence on the gap between the body and the contact plate and the actual gap is maintained about 19.8 [mm].

Finally, without the 19.8 mm gap, total size of the CHM is $44.8 \times 25.0 \times 19.4$ mm^3, and weight is about 23 [g] including three dc-micromotors (a single motor weight is 5 g), springs, wires, one FSR sensor, three soft sensors, and three-dimensional (3-D) printed parts (c.f., 32 [g], $48.8 \times 40.2 \times 21.5$ mm^3 of [23]). We also modularize the body and contact plate parts to be easily repaired or replaced.

B. Three-DOF Contact Force Rendering With the CHM

1) Closed-Loop Control of the CHM: The CHM displays a desired three-DOF contact force at the finger-tip (i.e., normal and planar shear forces) by pulling of its contact plate, which is placed under the finger-tip (see Fig. 5). Therefore, it is important to place the contact plate in an appropriate rotation and to regulate its pushing force magnitude. In this regard, the control problem is to generate the tensions of three wires

$$u := \begin{bmatrix} u_1; & u_2; & u_3 \end{bmatrix} \in \Re^3 \tag{3}$$

by three DC-micromotors to rotate and pull the contact plate to be aligned with a desired force direction (i.e., pitch/roll) with a desired force magnitude.

To analyze and derive the control of our three-DOF CHM, we first attach the frame $\{B\}$ to the body part and $\{C\}$ to the contact plate. We also denote vertexes of each triangle by $\mathcal{V}_{B_i}$ and $\mathcal{V}_{C_i}$, $i = (1, 2, 3)$, with their position vectors to be $p^B_{O_B,\mathcal{V}_{B_i}} \in \Re^3$ and $p^C_{O_C,\mathcal{V}_{C_i}} \in \Re^3$ expressed in the $\{B\}$-frame and the $\{C\}$-frame, respectively (see Figs. 5 and 6). To design the control $u \in \Re^3$ in (3), we also assume that the relative motion of the contact plate w.r.t. the body part can be well-represented by $\xi := [p_3; \theta_1; \theta_2] \in \Re^3$, where $p_3 := e_3^T p^B_{O_B,O_C}$ is the projection of the relative translation $p^B_{O_B,O_C}$ projected onto the e_3-direction, and θ_1, θ_2 are the roll and pitch angles of the contact plate relative to the $\{B\}$-frame. Even if the contact plate can in general assume six-DOF motion relative to the $\{B\}$-frame, we found this reduced three-DOF ξ-motion description can still adequately describe its motion, since, with the plate in contact with the finger-tip (as enforced by our control designed below), the horizontal translations (i.e., along e_1/e_2-directions) and the yaw angle (i.e., rotation along e_3-direction) of the plate is much less than this ξ-motion.

Now, suppose that a desired finger-tip feedback force $f^B_d \in \Re^3$ expressed in the $\{B\}$-frame is given from some VR simulation. The control objective can then be written as

$$(\theta_1, \theta_2) \to \text{vec}(f^B_d),\ \lambda_N \to \lambda_{N,d} \tag{4}$$

where λ_N is the force magnitude measured by the FSR sensor, which is normal to the surface of the contact plate, $\lambda_{N,d} := \|f^B_d\|$, (θ_1, θ_2) are the roll and pitch angles of the contact plate, and $\text{vec}(f^B_d) = (\theta^d_1, \theta^d_2)$ is the direction of f^B_d relative to the $\{B\}$-frame as captured by the roll and pitch angles, θ^d_1, θ^d_2.

To attain this control objective (4), we first design the control action for the contact plate along its reduced ξ-motion (i.e., force along the e_3-direction and moments along the roll/pitch angles) by

$$\tau^B_d = -K_P e_\gamma - K_I \int_0^t e_\gamma d\sigma \tag{5}$$

with

$$e_\gamma := \left[S_\gamma(\lambda_N - \lambda_{N,d}); \theta_1 - \theta^d_1; \theta_2 - \theta^d_2\right] \in \Re^3$$

where $S_\gamma := e_3^T R^B_{BC,d} e_3 \in \Re$ with $R^B_{BC,d} = \exp(\theta^d_2 e_2) \cdot \exp(\theta^d_1 e_1) \in \text{SO(3)}$, and $K_P, K_I \in \Re^{3\times3}$ are the positive-definite proportional and integral control gain matrices. Here, S_γ is first to assign $\lambda_N - \lambda_{N,d}$ along the normal (i.e., e_3) direction of the contact plate, and then project it along the e_3-direction of the $\{B\}$-frame (i.e., along the direction of p_3), whereas the second and third components of e_γ are along the directions of θ_1, θ_2, thereby, producing the control action along the (permissible) ξ-motion. This control action w.r.t. the contact plate is then mapped to the desired tension $u \in \Re^3$ in (3) of the three wires s.t.

$$u = J^{-1}(\xi)\tau^B_d \tag{6}$$

where $J(\xi) \in \Re^{3\times3}$ is the Jacobian matrix from $(\dot{l}_1, \dot{l}_2, \dot{l}_3)$ (i.e., length change rate of the three wires with l_i being the distance between $\mathcal{V}_{B_i}$ and $\mathcal{V}_{C_i}$) to $\dot{\xi} = (\dot{p}_3; \dot{\theta}_1; \dot{\theta}_2)$, which is always invertible since, in practice, $|\theta_2| < 90°$.

Here, note from Fig. 5 that the contact plate is actuated by the wires [i.e., u in (6)], yet, at the same time, it also experiences the resistive force from the springs, which are adopted to spare the space for the finger-tip. To compensate for this spring force, we add the corrective term to (6) s.t.

$$u' = u + K_s \Delta l$$

where $K_s \in \Re^{3\times3}$ is the (identified/known) diagonal and positive-definite spring stiffness matrix, and $\Delta l = l_o - l \in \Re^3$ is the spring deformation, where $l = [l_1; l_2; l_3]$ and $l_o = [l^1_o, l^2_o, l^3_o]$ are respectively the length between the vertexes $\mathcal{V}_{B_i}$ and $\mathcal{V}_{C_i}$ (measured by the soft sensor—see Fig. 5) and the initial length of the springs with $l^i_o > l_i$.

It is worthwhile to mention that our control (6) with (5) for the CHM is closed-loop control with feedback PI-action. This substantially improves the control performance and robustness against some such important phenomena inherent to our CHM as friction, soft sensor impedance, finger-tip stiffness, etc. Furthermore, this robustness allows us to overcome the user variability (e.g., difference in finger-tip size, shape, stiffness, manner of wearing device, etc.), one of the key challenges in any human-interactive robots and devices. This is in a stark contrast to other works on similar tendon-driven cutaneous haptic feedback devices (e.g., [21], [23]), where, typically, open-loop control based on some model (e.g., finger-tip stiffness model [21]) is adopted.

2) Pose Estimation of the Contact Plate: For the CHM tension control $u \in \Re^3$ in (6) with (5), we need to know the (reduced) ξ-pose of the contact plate relative to the body $\{B\}$-frame. Although, to compute (6), we only need θ_1, θ_2 (i.e., only attitude), here, we estimate $\xi = [p_3, \theta_1, \theta_2]$ all at the same time, since the computation cost increase is rather minimal. For this, we utilize custom-built resistive type soft sensors [35] to measure $l = [l_1; l_2; l_3]$, where $l_i \approx \|p^B_{\mathcal{V}_{B_i},\mathcal{V}_{C_i}}\|$ under the assumption of the reduced ξ-motion of the contact plate in Section II-B1. We adopt here the soft sensors instead of IMU sensors (e.g., [13], [37]) or three FSR sensors with finger-tip stiffness model (e.g., [21]), since each is fundamentally susceptible to IMU-motor electromagnetic interference or robustness issue stemming from the user variability and continuous-contact with all three FSR sensors.

The analytic expression of the "forward" kinematics from the lengths l to the ξ-pose is fairly complicated. The number of unknown (i.e., $\xi = [p_3; \theta_1; \theta_2] \in \Re^3$) is yet only three. Due to these reasons, in this paper, we formulate the ξ-pose estimation problem as a numerical problem and solve it with the Newton–Raphson algorithm. For this, consider the following kinematics relation:

$$p^B_{\mathcal{V}_{B_i},\mathcal{V}_{C_i}}(\xi) = \left(R^B_{BC} p^C_{O_C,\mathcal{V}_{C_i}} + p^B_{O_B,O_C}\right) - p^B_{O_B,\mathcal{V}_{B_i}}$$

where $R^B_{BC} = \exp(\xi_3 e_2) \cdot \exp(\xi_2 e_1)$ is the relative rotation (with zero yaw angle), $p^B_{O_B,O_C} = [0; 0; \xi_1]$ is the relative distance, and $p^B_{O_B,\mathcal{V}_{B_i}}, p^C_{O_C,\mathcal{V}_{C_i}}$ are the constant position vectors.

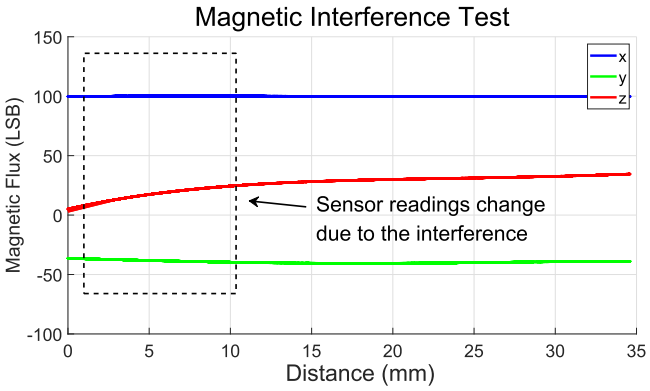

Fig. 7. By using 3-D printed mock-up and changing the relative distance and rotation between IMUs and dc-micromotors, magnetic interference is evaluated by observing sensor measurements. Sensor measurements changes when the distance between the motor and the IMU becomes closer. However, it is observed that the interference is only significant if the distance is less than 1 cm.

Now, define $h_i(\xi) := l_i^2 \approx ||p^B_{\mathcal{V}_{B_i}\mathcal{V}_{C_i}}(\xi)||^2$. We then have

$$\Delta h_i = 2p^{B,T}_{\mathcal{V}_{B_i},\mathcal{V}_{C_i}} \Delta p^B_{\mathcal{V}_{B_i},\mathcal{V}_{C_i}} = 2p^{B,T}_{\mathcal{V}_{B_i},\mathcal{V}_{C_i}} \sum_{j=1}^{3} \frac{\partial p^B_{\mathcal{V}_{B_i},\mathcal{V}_{C_i}}}{\partial \xi_j}\bigg|_{\xi_o} \Delta\xi_j$$

and, collecting these, we have

$$\Delta h = [\Delta h_1; \Delta h_2; \Delta h_3] = Q(\xi_o)\Delta\xi \tag{7}$$

where $Q(\xi_o) \in \Re^{3\times 3}$. From (7), we can then construct the Newton–Rahpson algorithm s.t.

$$\xi_{k+1} = \xi_k + Q^{-1}(\xi_k)(h(l_k) - h(\xi_k)) \tag{8}$$

where $Q(\xi)$ is numerically verified to be invertible for all possible ξ.

IV. Wearable Cutaneous Haptic Interface With Performance Evaluation

So far, we introduce the hardware configuration and its estimation/control of FTM and CHM. In Fig. 2, the integrated WCHI is presented with its two modules. The integration is achieved by attaching the CHM to the finger-tip of the glove of the FTM since both modules do not interfere functionally and mechanically with each other. Here, the functional interference (i.e., electromagnetic interference between IMUs and dc-micromotors) is validated experimentally as shown in Fig. 7. For this, we make a 3-D printed mock-up where the motor is fixed with different orientations (i.e., 0°, 45°, and 90°) and the MEMS IMU moves along a fixed trajectory. We measure the relative distance with MOCAP and the IMU's magnetic flux readings, and deduce the safe distance to be above 10 mm, which is incorporated on the design of each module and the integration for WCHI. Note that this safe distance is guaranteed even during full folding the fingers since the CHMs, thus dc-micromotors, are on the finger-tips while IMUs are on the proximal phalanges.

We also utilize two MCU boards (e.g., Arduino Nano) for the data acquisition of each IMUs and soft sensors of the FTM,

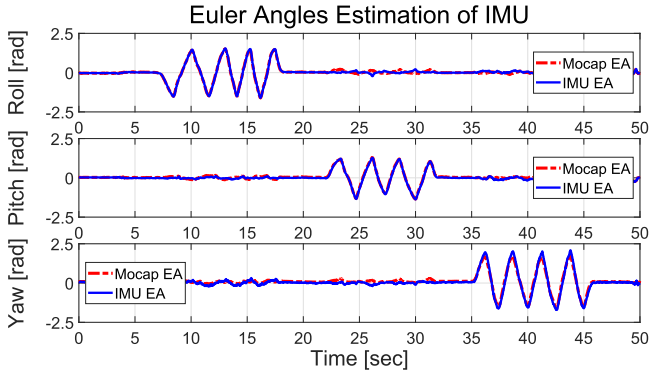

Fig. 8. Comparison of ZYX EA of the IMU in Section II-B2. Reference EAs are captured from MOCAP and palm-shaped 3D printed mock-up. The mean angle error is 1.567°.

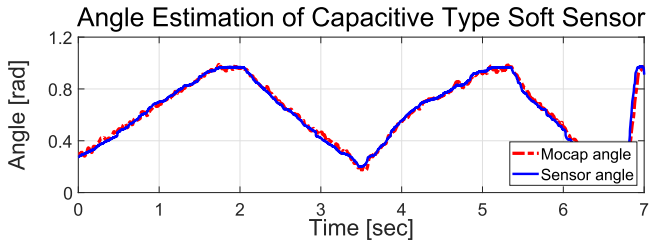

Fig. 9. Comparison of single-DOF joint angle tracking of the soft sensor utilized in Section II-B2. The reference joint angle is captured from MOCAP and index-finger-shaped 3-D printed mock-up. The mean angle error is 0.0685°.

which run at 200 and 1 kHz, respectively. One MCU board (i.e., Arduino Uno with the Adafruit Motor Shield V2 and standard op-amp circuit for sensor signal) is also employed for the control and the data acquisition of the CHM, which runs at 120 Hz.

A. Quantitative Evaluation

To precisely evaluate the performance of the FTM and the CHM, we make 3-D printed mock-ups while employing the motion capture system (Optitrack) for the ground truth data acquisition. For the performance evaluation of the FTM, we first check the rotation estimation performance of the IMU. We rotate the IMU about 90° with respect to *X/Y/Z*-axes directions, respectively, to clearly check roll/pitch/yaw angle estimations, while attaching IR-markers for the MOCAP rotation tracking. In Fig. 8, we display the rotation tracking performance of the IMU expressed by the Euler angle (EA). The mean EA estimation error compared to the MOCAP is given as 1.567°. The small error may be originated from the imperfect calibration of the IMU [38] and the latency of SO(3) filter [33] which we use. On the other hand, as shown in Fig. 9, we show that the single-DOF joint angle tracking performance of the capacitive-type soft sensor employed, e.g., for the PIP joint of index finger, we achieved 0.0685° mean error where the small error mainly comes from the signal noise and the delay due to the first-order low-pass filter we used to reduce that noise. While propagating these errors with the middle finger length in [39] (i.e., total 10.5 cm), the finger-tip position error would be 0.15 cm and less

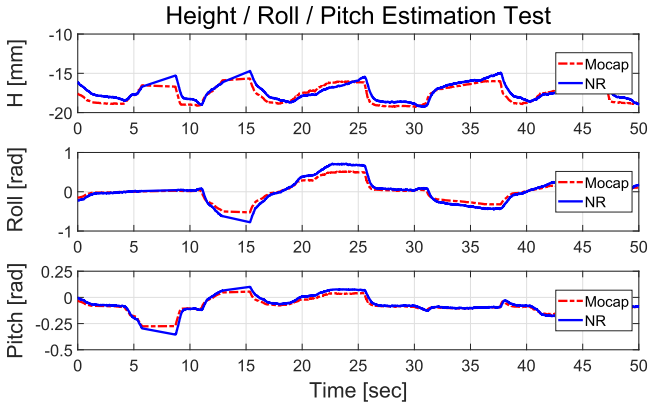

Fig. 10. Comparison of height/roll/pitch estimation performance of the Newton–Raphson method in Section III-B. The height/roll/pitch estimation values obtained from the Newton–Raphson method are marked as "NR" while the reference values obtained from the MOCAP are marked as "Mocap."

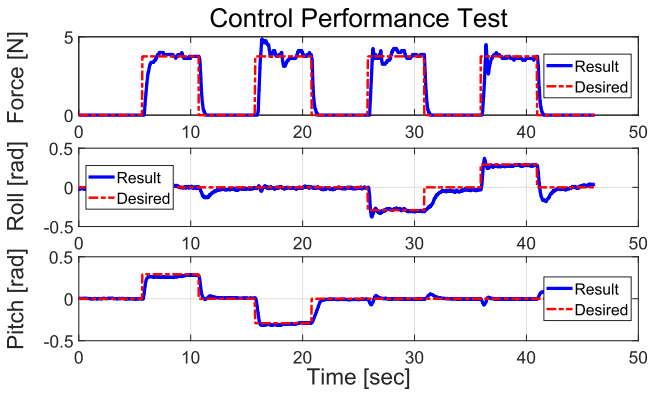

Fig. 11. Contact force and its roll/pitch directions tracking performance of the proposed controller (6). The measured force/roll/pitch values converge to the desired value.

than 3.64 cm, which is the indistinguishable threshold under haptic feedback in VR [37].

Meanwhile, in Figs. 10 and 11, we compare the three-DOF relative position/rotation estimation and its cutaneous feedback rendering of the CHM in Section III-B. Due to the underactuation of the wire-driven CHM, there is an error between estimated height/roll/pitch values and reference values obtained from the MOCAP data as shown in Fig. 10. The mean errors are 0.597 mm in height, 3.74° in roll, and 0.919° in pitch, respectively. The error in roll is larger than that of pitch, since the pitch angle affects the roll angle estimation in the ZYX EA parametrization. Note that the error becomes larger with large rotation since the more the contact plate inclines, the more translation along e_1/e_2-directions and yaw rotation, which results in inaccuracy in three-DOF reduced model, takes place. However, the tendency is strongly marked as shown in Fig. 10, which implies that the current three-DOF model assumption in Section III-B is effective. Therefore, we believe that we can further improve the current estimation performance by, for example, employing a more sophisticated estimation technique such as machine learning over the Newton–Raphson based estimation. We left this as a future research topic.

On the other hand, for the estimated ξ of (8), the proposed control (6) can robustly track the contact force magnitude and the plate rotation as shown in Fig. 11. In the experiment, we use K_P = (50, 750 N·mm, 1500 N·mm) and K_I = (300, 900 N·mm, 1800 N·mm) with the saturation technique to cope with the error accumulation of the integral control. Finally, the normal pushing force is measured to be maximum about 10 N, which purely translates to the user as haptic feedback.

B. Usability Evaluation

Now, we conduct the user study to assess the effectiveness of the WCHI for VR application. We emulate a virtual manipulation task, inserting a breakable peg into a horizontally placed hole as shown in Fig. 12. The peg is 186.2 mm in height, 25.84 mm in radius, and 500 g in weight, which models a round bottle as a daily object. This peg inserting task is chosen here since, to manipulate its attitude and do the task, more complex finger control is required. All the subjects also attempt finger-tip manipulation, instead of power grasping, since it is fairly difficult to properly control the motion and insertion force without no haptic feedback on the palm. Our hypothesis is that the AA motion will be more important for this kind of real-life like complex task as compared to, e.g., the needle insertion [21] or the delivery task of simple object such as an egg, since the peg attitude should be controlled precisely to be inserted. On the other hand, we set the peg to be broken with large contact force (i.e., $\geq$5 N). Therefore, subjects have to utilize the haptic feedback, even though it only exists at finger-tips, to successfully perform the task. The virtual hand is then controlled via the virtual coupling technique [40] where the desired hand motion is obtained from the FTM. The three-DOF contact force between the virtual hand and peg is fed back through CHM. Consequently, the test setup consists of WCHI, Oculus Rift HMD, soundproof earmuffs, and two HTC VIVE trackers to locate global position of a wrist and HMD, respectively, in a designated space as shown in Fig. 1.

1) Methods: We design four different test settings to evaluate the performance of WCHI, especially the importance of the three-DOF cutaneous haptic feedback and the AA tracking motion of a hand for the VR application since typical VR hand interfaces have at best single-DOF haptic feedback and/or hand tracking without AA motion (e.g., MANUS VR glove, etc.). We intentionally turn ON and OFF the actuation for with and without cutaneous haptic feedback (wHF or woHF) from CHM, and also turn ON and OFF the allowance of AA tracking motion (wAA or woAA) of the FTM during the tests. As a result, the four settings are: 1) wHF wAA, 2) wHF woAA, 3) woHF wAA, and 4) woHF woAA. We then measure the task completion time for each trial and consider it as a performance measurement of the given task.

Then, the user study procedure consists of two phases: 1) familiarization and 2) main task. During the familiarization, we introduced WCHI to users and verbally explain overall information about the task. We informed that there were four different settings, yet we did not provide details of each setting, not to make presuppose superiority and/or inferiority of each setting and try to distinguish them intentionally. Here, we also calibrate

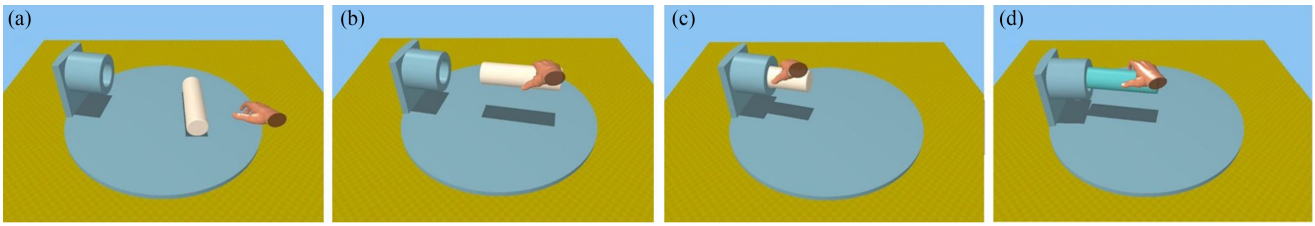

Fig. 12. We conduct the usability evaluation with the virtual manipulation task of inserting a breakable peg into a horizontally placed hole: For each trial, we randomly change both the initial starting point of the peg and location of the hole (a). Then, a subject picks up and manipulates the peg to do the insertion task (b). During the insertion task (c), the subject can see whether the peg is broken or not with the change of its color (d).

the WCHI, especially the FTM, to fit each subject's hand motion as in Section II-B.

After the explanation and calibration, the 6 min of familiarization phase consists of two scenarios to gradually learn about the WCHI and HMD worn VR environment. For the first 3 min, users were instructed to touch and grasp the peg, which is suspended in the air by spring, and feel corresponding haptic feedback. We set the breaking force threshold of peg to be 5 N (i.e., $0 \leq |\lambda_N| \leq 10$ [N]) and change the peg color from white to blue [see Fig. 12(d)]. Users can learn an appropriate grasping force by matching the visual information and haptic feedback. In the next 3 min, users were asked to gently lift and rotate the peg from the ground to become accustomed to the peg manipulation with different hand postures. Throughout this phase, we provided users the full haptic feedback and hand tracking, i.e., setting 1 (wHF and wAA).

After that, each user experienced total 20 main tasks with repeated four different randomized settings for five times to minimize the learning effect. We also randomly (yet not too much) change the hole position and the starting point of the peg, again to minimize the learning effect. During the task, once the peg is broken down, it has to move back to a starting point while task time is continuously running. One thing to mention here is that we considered first four tasks as an extension of familiarization phase for the main task. Thus, we took account the results of last 16 tasks as a valid data for the analysis.

Ten users participated in the study including nine male and one female in average 25.3 $\pm$ 2.0 years old. All of them were right-hand users except two. All users did not have any physical or mental difficulty to complete the given test.

2) Result and Discussion: To evaluate the difference between each setting, we collected in total 160 trials data from ten users. The normalized mean time and standard deviation of ten users for each setting are depicted in Fig. 13. As a result, the normalized mean time of setting 1 (0.678) takes about 2.1 times less than that of setting 4 (1.414). Also, the standard deviation of setting 1 (0.176) is 4.8 times less than that of setting 4 (0.838). On the other hand, the normalized mean time and the standard deviation of setting 2 (0.939 $\pm$ 0.488) and setting 3 (0.969 $\pm$ 0.507), where neither one of the conditions was not allowed, do not show significant difference. Both setting 2 and setting 3 take less time than setting 4 while taking more time than setting 1.

In further analysis, the normalized time is tested with one-way repeated measures ANOVA with the Greenhouse–Geisser correction ($\epsilon = 0.672$). The analysis determines that the normalized time has statistically significant difference between four settings on the peg-in-hole task, ($F(2.018, 78.684) = 13.076$,

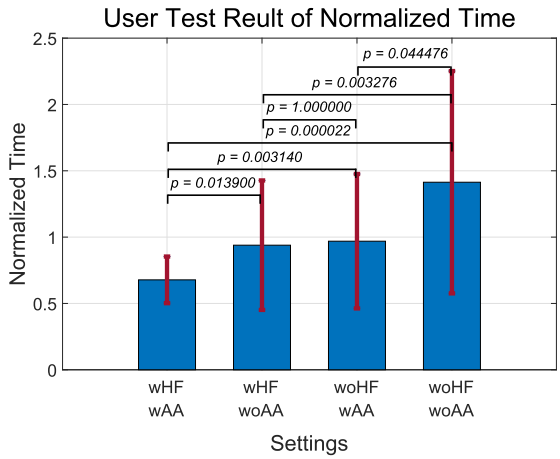

Fig. 13. Normalized mean time and standard deviation results of ten users according to four different settings. Post hoc tests using the Bonferroni method revealed that there exists statistically significant difference between each setting except between setting 2 and setting 3 ($p = 1.000$).

$p = 0.000012$). Post hoc tests using the Bonferroni method revealed that there exists statistically significant difference between each setting except between setting 2 and setting 3 as shown in Fig. 13. This result does not change when we employ the Holm–Bonferroni method, which is known to be less conservative than the Bonferroni method. This is because, for our post hoc test, the p-value between setting 2 and setting 3 is 1 (i.e., $p = 1.000$). We illustrate every p-value between the four settings in Fig. 13.

We can understand above results and educe some insight for VR manipulation. First of all, on VR environment, each user uses and is affected by different conditions (or information). Three users are more likely to be affected by the role of haptic feedback than AA tracking motion. We called them haptic feedback oriented users. These users tend to depend more on haptic feedback on or off conditions than the existence of AA tracking motion to complete the trials. Conversely, two users were affected by the role of AA tracking motion than haptic feedback, we called them AA tracking oriented users. These users depend more on allowance of the AA tracking motion on VR manipulation than haptic feedback. Rest users do get affected by both conditions similarly. Fig. 14 is a representative example for each oriented case. Above all, all ten users still performed consistently best with setting 1 where both haptic feedback and AA motion are provided. This result clearly shows that both haptic feedback and AA tracking motion are important for the virtual manipulation task.

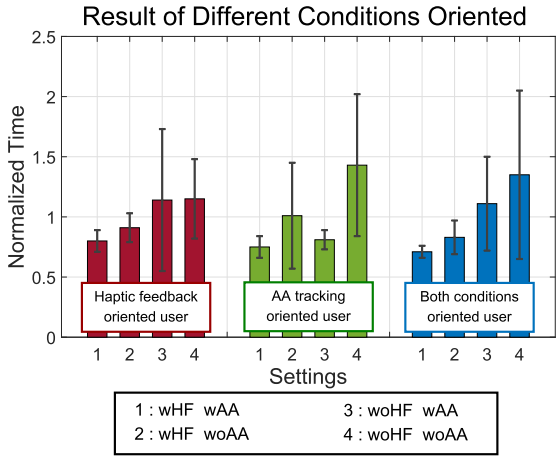

Fig. 14. Normalized mean time and standard deviation results of haptic feedback oriented user (user 5, Left), AA tracking motion oriented user (user 4, middle), and both condition oriented user (user 9, right). Here, "oriented" indicates an influence of one setting over other setting on user (e.g., more affect by haptic feedback than AA tracking motion and vice versa).

Second, when we compare the haptic feedback and the AA motion, the difference in p-value size can be interpreted that the haptic feedback is more likely to be effective than the AA motion. For example, the p-value between setting 3 and setting 4 is 0.044476, which is larger and similar to the significance level while the p-value between setting 2 and setting 4 is 0.003276. This tendency is also found when we compare setting 2 and setting 3 to setting 1. This interpretation is consistent with the research context that many studies have focused more on the haptic feedback than on the AA motion, and can be an explanation of why the AA motion gets less attention for a hand interface while the haptic feedback is often pointed out for constructing immersive and informative VR interaction.

V. Conclusion

In this paper, we introduce novel FTM and CHM, and their integration to WCHI for wearable multi-fingered haptic interaction for VR. Both the FTM and the CHM are based on the heterogeneous sensors (i.e., soft sensors, IMUs, FSR sensors), which allow for multi-DOF anatomically consistent dexterous finger/hand motion tracking while avoiding motor-IMU magnetic interference and high-performance/robust generation of three-DOF cutaneous finger-tip haptic feedback against uncertainty, friction, unmodeled compliance and user variability. We present the design, implementation, analysis, and algorithms for the FTM and CHM, and also conduct human subject study to verify the performance/capability of our proposed WCHI, particularly the importance of haptic feedback and full motion tracking it conveys for application where dexterity and complexity of finger/hand motion are involved.

Some future research directions are as follows.

1) Onboard implementation of our proposed WCHI with wireless communication, onboard power and computing.
2) Combination of our WCHI with simultaneous localization and mapping for untethered VR applications.
3) Applications of our WCHI for other VR scenarios (e.g., multi-user collaborative haptic manipulation [41]).
4) Various human perception study in VR environment using WCHI, particularly, to set the device specification [37].

Acknowledgment

This authors would like to thank to Mr. G. Shin for his help in preparing for using soft sensors of Section III and also thank to all participants in usability evaluation of Section IV-B.

References

[1] I. Oikonomidis, N. Kyriazis, and A. A. Argyros, "Efficient model-based 3d tracking of hand articulations using kinect," in *Proc. Brit. Mach. Vis. Conf.*, 2011, pp. 101.1–101.11.
[2] J.-S. Kim and J.-M. Park, "Physics-based hand interaction with virtual objects," in *Proc. IEEE Int. Conf. Robot. Automat.*, 2015, pp. 3814–3819.
[3] L. Meli, S. Scheggi, C. Pacchierotti, and D. Prattichizzo, "Wearable haptics and hand tracking via an rgb-d camera for immersive tactile experiences," in *Proc. ACM SIGGRAPH Posters*, 2014, p. 56.
[4] M. Maisto, C. Pacchierotti, F. Chinello, G. Salvietti, A. De Luca, and D. Prattichizzo, "Evaluation of wearable haptic systems for the fingers in augmented reality applications," *IEEE Trans. Haptics*, vol. 10, no. 4, pp. 511–522, Oct./Dec. 2017.
[5] A. G. Perez, G. Cirio, D. Lobo, F. Chinello, D. Prattichizzo, and M. A. Otaduy, "Efficient nonlinear skin simulation for multi-finger tactile rendering," in *Proc. IEEE Haptics Symp.*, 2016, pp. 155–160.
[6] "Cyber glove systems." 1990. [Online]. Available: http://www.cyberglovesystems.com/
[7] L. Cui, U. Cupcic, and J. S. Dai, "An optimization approach to teleoperation of the thumb of a humanoid robot hand: Kinematic mapping and calibration," *J. Mech. Design*, vol. 136, no. 9, 2014, Art. no. 091005.
[8] W. Park, K. Ro, S. Kim, and J. Bae, "A soft sensor-based three-dimensional (3-d) finger motion measurement system," *Sensors*, vol. 17, no. 2, 2017, Art. no. 420.
[9] J.-B. Chossat, Y. Tao, V. Duchaine, and Y.-L. Park, "Wearable soft artificial skin for hand motion detection with embedded microfluidic strain sensing," in *Proc. IEEE Int. Conf. Robot. Automat.*, 2015, pp. 2568–2573.
[10] D. H. Kim, S. W. Lee, and H.-S. Park, "Improving kinematic accuracy of soft wearable data gloves by optimizing sensor locations," *Sensors*, vol. 16, no. 6, 2016, Art. no. 766.
[11] "Perception neuron." 2011. [Online]. Available: https://neuronmocap.com/
[12] G. Santaera, E. Luberto, A. Serio, M. Gabiccini, and A. Bicchi, "Low-cost, fast and accurate reconstruction of robotic and human postures via IMU measurements," in *Proc. IEEE Int. Conf. Robot. Automat.*, 2015, pp. 2728–2735.
[13] T. L. Baldi, M. Mohammadi, S. Scheggi, and D. Prattichizzo, "Using inertial and magnetic sensors for hand tracking and rendering in wearable haptics," in *Proc. IEEE World Haptics Conf.*, 2015, pp. 381–387.
[14] M. Mohammadi, T. L. Baldi, S. Scheggi, and D. Prattichizzo, "Fingertip force estimation via inertial and magnetic sensors in deformable object manipulation," in *Proc. IEEE Haptics Symp.*, 2016, pp. 284–289.
[15] J. Q. Coburn, I. Freeman, and J. L. Salmon, "A review of the capabilities of current low-cost virtual reality technology and its potential to enhance the design process," *J. Comput. Inf. Sci. Eng.*, vol. 17, 2017, Art. no. 031013.
[16] D. Prattichizzo, C. Pacchierotti, and G. Rosati, "Cutaneous force feedback as a sensory subtraction technique in haptics," *IEEE Trans. Haptics*, vol. 5, no. 4, pp. 289–300, Fourth Quarter 2012.
[17] I. Jang and D. J. Lee, "On utilizing pseudo-haptics for cutaneous fingertip haptic device," in *Proc. Haptics Symp.*, 2014, pp. 635–639.
[18] Z. F. Quek, S. B. Schorr, I. Nisky, W. R. Provancher, and A. M. Okamura, "Sensory substitution and augmentation using 3-degree-of-freedom skin deformation feedback," *IEEE Trans. Haptics*, vol. 8, no. 2, pp. 209–221, Apr./Jun. 2015.
[19] K. Minamizawa, S. Fukamachi, H. Kajimoto, N. Kawakami, and S. Tachi, "Gravity grabber: Wearable haptic display to present virtual mass sensation," in *Proc. ACM SIGGRAPH Emerging Technol.*, 2007, Art. no. 8.
[20] D. Prattichizzo, C. Pacchierotti, S. Cenci, K. Minamizawa, and G. Rosati, "Using a fingertip tactile device to substitute kinesthetic feedback in haptic interaction," in *Haptics: Generating and Perceiving Tangible Sensations*. New York, NY, USA: Springer, 2010, pp. 125–130.

[21] D. Prattichizzo, F. Chinello, C. Pacchierotti, and M. Malvezzi, "Towards wearability in fingertip haptics: A 3-dof wearable device for cutaneous force feedback," *IEEE Trans. Haptics*, vol. 6, no. 4, pp. 506–516, Oct./Dec. 2013.
[22] D. Leonardis, M. Solazzi, I. Bortone, and A. Frisoli, "A wearable fingertip haptic device with 3 dof asymmetric 3-rsr kinematics," in *Proc. IEEE World Haptics Conf.*, 2015, pp. 388–393.
[23] S. B. Schorr and A. Okamura, "Three-dimensional skin deformation as force substitution: Wearable device design and performance during haptic exploration of virtual environments," *IEEE Trans. Haptics*, vol. 10, no. 3, pp. 418–430, Jul./Sep. 2017.
[24] P. Weber, E. Rueckert, R. Calandra, J. Peters, and P. Beckerle, "A low-cost sensor glove with vibrotactile feedback and multiple finger joint and hand motion sensing for human-robot interaction," in *Proc. IEEE Int. Symp. Robot Human Interactive Commun.*, 2016, pp. 99–104.
[25] "Manus vr." [Online]. Available: https://manus-vr.com/
[26] L. Y. Chang and N. S. Pollard, "Method for determining kinematic parameters of the in vivo thumb carpometacarpal joint," *IEEE Trans. Biomed. Eng.*, vol. 55, no. 7, pp. 1897–1906, Jul. 2008.
[27] A. Hollister, D. J. Giurintano, W. L. Buford, L. M. Myers, and A. Novick, "The axes of rotation of the thumb interphalangeal and metacarpophalangeal joints," *Clin. Orthopaedics Related Res.*, vol. 320, pp. 188–193, 1995.
[28] K. Kim, Y. Youm, and W. K. Chung, "Human kinematic factor for haptic manipulation: The wrist to thumb," in *Proc. Haptics Symp. Haptic Interfaces Virtual Environ. Teleoperator Syst.*, 2002, pp. 319–326.
[29] C.-E. Hrabia, K. Wolf, and M. Wilhelm, "Whole hand modeling using 8 wearable sensors: Biomechanics for hand pose prediction," in *Proc. 4th Augmented Human Int. Conf.*, 2013, pp. 21–28.
[30] A. D. Deshpande *et al.*, "Mechanisms of the anatomically correct testbed hand," *IEEE/ASME Trans. Mechatronics*, vol. 18, no. 1, pp. 238–250, Feb. 2013.
[31] M. Chalon, M. Grebenstein, T. Wimböck, and G. Hirzinger, "The thumb: Guidelines for a robotic design," in *Proc. IEEE/RSJ Int. Conf. Intell. Robots Syst.*, 2010, pp. 5886–5893.
[32] L. Y. Chang and Y. Matsuoka, "A kinematic thumb model for the act hand," in *Proc. IEEE Int. Conf. Robot. Automat*, 2006, pp. 1000–1005.
[33] R. Mahony, T. Hamel, and J.-M. Pflimlin, "Nonlinear complementary filters on the special orthogonal group," *IEEE Trans. Autom. Control*, vol. 53, no. 5, pp. 1203–1218, Jun. 2008.
[34] R. M. Murray, Z. Li, and S. S. Sastry, *A Mathematical Introduction to Robotic Manipulation*. Boca Ranton, FL, USA: CRC Press, 1993.
[35] Y.-L. Park, B.-R. Chen, and R. J. Wood, "Design and fabrication of soft artificial skin using embedded microchannels and liquid conductors," *IEEE Sensors J.*, vol. 12, no. 8, pp. 2711–2718, Aug. 2012.
[36] A. Spring, *Design Handbook: Engineering Guide to Spring Design*. Bristol, CT, USA: Associated Spring, Barnes Group Inc., 1981.
[37] Y. Lee, I. Jang, and D. Lee, "Enlarging just noticeable differences of visual-proprioceptive conflict in vr using haptic feedback," in *Proc. World Haptics Conf.*, 2015, pp. 19–24.
[38] F. L. Markley, "Attitude determination using vector observations and the singular value decomposition," *J. Astronautical Sci.*, vol. 36, no. 3, pp. 245–258, 1988.
[39] M. Peters, K. Mackenzie, and P. Bryden, "Finger length and distal finger extent patterns in humans," *Am. J. Phys. Anthropology*, vol. 117, no. 3, pp. 209–217, 2002.
[40] M. Kim, Y. Lee, Y. Lee, and D. J. Lee, "Haptic rendering and interactive simulation using passive midpoint integration," *Int. J. Robot. Res.*, vol. 36, no. 12, pp. 1341–1362, 2017.
[41] K. Huang and D. J. Lee, "Consensus-based peer-to-peer control architecture for multiuser haptic interaction over the internet," *IEEE Trans. Robot.*, vol. 29, no. 2, pp. 417–431, Apr. 2013.

Yongjun Lee received the B.S. degree in mechanical engineering from Hanyang University, Seoul, South Korea, in 2013 and the M.S. degrees both in product design from Hongik University, Seoul, South Korea, in 2016, and in mechanical engineering from Seoul National University, Seoul, South Korea, in 2018.

He is currently with Harnics for alternative military service. His research interests include wearable haptics and vision guided robotics.

Myungsin Kim received the B.S. degree in mechanical and aerospace engineering from Seoul National University, Seoul, South Korea, in 2011. He is currently working toward the Ph.D. degree in mechanical engineering with Seoul National University.

His research interests include passivity based haptic rendering and control, wearable haptics, and network-based multiuser haptics.

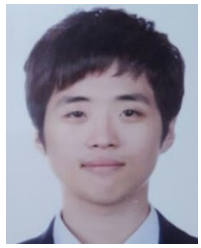

Yongseok Lee received the B.S. degree in mechanical and aerospace engineering from Seoul National University, Seoul, South Korea, in 2013. He is currently working toward the Ph.D. degree in mechanical engineering with Seoul National University.

His current research interests include wearable hand tracking systems and state estimation for aerial robots.

Junghan Kwon received the B.S. and M.S. degrees in naval architecture and ocean engineering from Seoul National University, Seoul, South Korea, in 2008 and 2010, respectively. He is currently working toward Ph.D. degree in mechanical engineering with Seoul National University.

His research interests include soft sensors, soft actuators, and soft wearable robots.

Yong-Lae Park received the M.S. and Ph.D. degrees in mechanical engineering from Stanford University, Stanford, CA, USA, in 2005 and 2010, respectively.

He is currently an Associate Professor with the Department of Mechanical Engineering, Seoul National University, Seoul, South Korea. Prior to joining SNU, he was an Assistant Professor with the Robotics Institute, Carnegie Mellon University, Pittsburgh, PA, USA (2013–2017). His current research interests include soft robots, artificial skin sensors and muscle actuators, and soft wearable robots and devices.

Dongjun Lee received the B.S. degree in mechanical engineering from Korea Advanced Institute of Science and Technology (KAIST), Daejeon, South Korea, the M.S. degree in automation and design from KAIST, Seoul, South Korea, and the Ph.D. degree in mechanical engineering from the University of Minnesota at Twin Cities, Minneapolis, MN, USA, in 2004.

He is currently a Professor with the Department of Mechanical and Aerospace Engineering, Seoul National University, Seoul, South Korea. His main research interests include dynamics and control of robotic and mechatronic systems with emphasis on teleoperation/haptics, aerial robots, multirobot systems, and industrial control applications.